Real-time Nyquist pulse generation beyond 100 Gbit/s and its relation to OFDM

R. Schmogrow,[1,*] M. Winter,[1,6] M. Meyer,[1] D. Hillerkuss,[1] S. Wolf,[1] B. Baeuerle,[1] A. Ludwig,[1] B. Nebendahl,[4] S. Ben-Ezra,[5] J. Meyer,[3] M. Dreschmann,[3] M. Huebner,[3] J. Becker,[3] C. Koos,[1,2] W. Freude,[1,2] and J. Leuthold[1,2]

[1]*Institute of Photonics and Quantum Electronics (IPQ), Karlsruhe Institute of Technology (KIT), Karlsruhe, Germany*
[2]*Institute of Microstructure Technology (IMT), Karlsruhe Institute of Technology (KIT), Karlsruhe, Germany*
[3]*Institute of Information Processing Technology (ITIV), Karlsruhe Institute of Technology (KIT), Karlsruhe, Germany*
[4]*Agilent Technologies, Boeblingen, Germany*
[5]*Finisar, Nes Ziona, Isreal*
[6]*Now with Polytec GmbH, Polytec-Platz 1-7, 76337 Waldbronn, Germany*
[*]*rene.schmogrow@kit.edu*

Abstract: Nyquist sinc-pulse shaping provides spectral efficiencies close to the theoretical limit. In this paper we discuss the analogy to optical orthogonal frequency division multiplexing and compare both techniques with respect to spectral efficiency and peak to average power ratio. We then show that using appropriate algorithms, Nyquist pulse shaped modulation formats can be encoded on a single wavelength at speeds beyond 100 Gbit/s in real-time. Finally we discuss the proper reception of Nyquist pulses.

OCIS codes: (060.4510) Optical communications; (060.1660) Coherent communications.

References and links

1. W. Shieh, H. Bao, and Y. Tang, "Coherent optical OFDM: theory and design," Opt. Express **16**(2), 841–859 (2008).
2. D. Hillerkuss, R. Schmogrow, T. Schellinger, M. Jordan, M. Winter, G. Huber, T. Vallaitis, R. Bonk, P. Kleinow, F. Frey, M. Roeger, S. Koenig, A. Ludwig, A. Marculescu, J. Li, M. Hoh, M. Dreschmann, J. Meyer, S. Ben Ezra, N. Narkiss, B. Nebendahl, F. Parmigiani, P. Petropoulos, B. Resan, A. Oehler, K. Weingarten, T. Ellermeyer, J. Lutz, M. Moeller, M. Huebner, J. Becker, C. Koos, W. Freude, and J. Leuthold, "26 Tbit s^{-1} line-rate super-channel transmission utilizing all-optical fast Fourier transform processing," Nat. Photonics **5**(6), 364–371 (2011).
3. X. Liu, S. Chandrasekhar, B. Zhu, P. Winzer, A. Gnauck, and D. Peckham, "448-Gb/s reduced-guard-interval CO-OFDM transmission over 2000 km of ultra-large-area fiber and five 80-GHz-grid ROADMs," J. Lightwave Technol. **29**(4), 483–490 (2011).
4. R. Schmogrow, M. Winter, M. Meyer, D. Hillerkuss, B. Nebendahl, J. Meyer, M. Dreschmann, M. Huebner, J. Becker, C. Koos, W. Freude, and J. Leuthold, "Real-time Nyquist pulse modulation transmitter generating rectangular shaped spectra of 112 Gbit/s 16QAM signals," in *Signal Processing in Photonic Communications*, OSA Technical Digest (CD) (Optical Society of America, 2011), paper SPMA5. *http://www.opticsinfobase.org/abstract.cfm?URI=SPPCom-2011-SPMA5*
5. M. Nakazawa, S. Okamoto, T. Omiya, K. Kasai, and M. Yoshida, "256 QAM (64 Gbit/s) coherent optical transmission over 160 km with an optical bandwidth of 5.4 GHz," in *Optical Fiber Communications Conference*, OSA Technical Digest (CD) (Optical Society of America, 2010), paper OMJ5. *http://www.opticsinfobase.org/abstract.cfm?URI=OFC-2010-OMJ5*
6. R. Essiambre, G. Kramer, P. Winzer, G. Foschini, and B. Goebel, "Capacity limits of optical fiber networks," J. Lightwave Technol. **28**(4), 662–701 (2010).
7. A. Ellis, J. Zhao, and D. Cotter, "Approaching the non-linear Shannon limit," J. Lightwave Technol. **28**(4), 423–433 (2010).
8. M. Sjödin, P. Johannisson, H. Wymeersch, P. A. Andrekson, and M. Karlsson, "Comparison of polarization-switched QPSK and polarization-multiplexed QPSK at 30 Gbit/s," Opt. Express **19**(8), 7839–7846 (2011).
9. H. Nyquist, "Certain topics in telegraph transmission theory," Trans. Am. Inst. Electr. Eng. **47**(2), 617–644 (1928).
10. G. Bosco, V. Curri, A. Carena, P. Poggiolini, and F. Forghieri, "On the Performance of Nyquist-WDM Terabit Superchannels Based on PM-BPSK, PM-QPSK, PM-8QAM or PM-16QAM Subcarriers," J. Lightwave Technol. **29**(1), 53–61 (2011).
11. D. Hillerkuss, R.Schmogrow, M. Meyer, S. Wolf, M. Jordan, P. Kleinow, N. Lindenmann, P. Schindler, A. Melikyan, X. Yang, S. Ben-Ezra, B. Nebendahl, M. Dreschmann, J. Meyer, F. Parmigiani, P. Petropoulos, B.

#158081 - $15.00 USD Received 14 Nov 2011; accepted 3 Dec 2011; published 20 Dec 2011

Resan, A. Oehler, K. Weingarten, L. Altenhain, T. Ellermeyer, M. Moeller, M. Huebner, J. Becker, C. Koos, W. Freude, and J. Leuthold, "32.5 Tbit/s 16QAM Nyquist – WDM transmission, Opt. Express (submitted).
12. Z. Dong, J. Yu, H. C. Chien, N. Chi, L. Chen, and G. K. Chang, "Ultra-dense WDM-PON delivering carrier-centralized Nyquist-WDM uplink with digital coherent detection," Opt. Express **19**(12), 11100–11105 (2011).
13. X. Zhou, L. Nelson, P. Magill, B. Zhu, and D. Peckham, "8x450-Gb/s, 50-GHz-spaced, PDM-32QAM transmission over 400km and one 50GHz-grid ROADM," in *Optical Fiber Communications Conference*, OSA Technical Digest (CD) (Optical Society of America, 2011), paper PDPB3. *http://www.opticsinfobase.org/abstract.cfm?URI=OFC-2011-PDPB3*
14. R. Schmogrow, D. Hillerkuss, M. Dreschmann, M. Huebner, M. Winter, J. Meyer, B. Nebendahl, C. Koos, J. Becker, W. Freude, and J. Leuthold, "Real-time software-defined multiformat transmitter generating 64QAM at 28 GBd," IEEE Photon. Technol. Lett. **22**(21), 1601–1603 (2010).
15. L. Lo Presti and M. Mondin, "Design of optimal FIR raised-cosine filters," Electron. Lett. **25**(7), 467–468 (1989).
16. E. Sun, B. Tian, Y. Wang, and K. Yi, "Quasi-orthogonal time division multiplexing and its applications under Rayleigh fading channels," in *Advanced Information Networking and Applications Workshops, 2007, 21st International Conference on* **1**, 172–176 (2007).
17. M. Abramowitz and I. A. Stegun, eds., "Exponential Integral and Related Functions," in *Handbook of Mathematical Functions* (Dover, New York, 1972), Eq. (5).2.1, p. 231.
18. R. Schmogrow, B. Nebendahl, M. Winter, A. Josten, D. Hillerkuss, J. Meyer, M. Dreschmann, M. Huebner, C. Koos, J. Becker, W. Freude, and J. Leuthold, "Error vector magnitude as a performance measure for advanced modulation formats," Photon. Technol. Lett., DOI: *10.1109/LPT.2011.2172405*.
19. I. S. Gradstein and I. M. Ryshik, eds., *Tables of Series, Products, and Integrals*, Vol. 1 and 2. (Harri Deutsch, Frankfurt, 1981).
20. P. Milder, R. Bouziane, R. Koutsoyannis, C. Berger, Y. Benlachtar, R. Killey, M. Glick, and J. Hoe, "Design and Simulation of 25 Gb/s Optical OFDM Transceiver ASICs," in *37th European Conference and Exposition on Optical Communications*, OSA Technical Digest (CD) (Optical Society of America, 2011), paper We.9.A.5. *http://www.opticsinfobase.org/abstract.cfm?URI=ECOC-2011-We.9.A.5*
21. R. Schmogrow, M. Winter, D. Hillerkuss, B. Nebendahl, S. Ben-Ezra, J. Meyer, M. Dreschmann, M. Huebner, J. Becker, C. Koos, W. Freude, and J. Leuthold, "Real-time OFDM transmitter beyond 100 Gbit/s," Opt. Express **19**(13), 12740–12749 (2011).
22. D. Rafique and A. D. Ellis, "Nonlinear penalties in long-haul optical networks employing dynamic transponders," Opt. Express **19**(10), 9044–9049 (2011).

1. Introduction

Sinc-shaped Nyquist pulses spread into adjacent time slots, but their rectangularly shaped spectra require only the minimum Nyquist channel bandwidth. They are well known from communication theory but are relatively new in optical communications. The Nyquist modulation format is very similar to optical orthogonal frequency division multiplexing (OFDM), where sinc-shaped sub-spectra extend into adjacent frequency slots, and symbols in time are rectangularly shaped. In the course of this paper all Nyquist pulses are sinc-shaped.

Here, we first discuss the close relation of Nyquist pulse modulation with OFDM [1–3]. Both Nyquist pulse shaping and OFDM are described with a similar formalism. This way it will become clear that Nyquist modulation is nothing but an orthogonal time division multiplexing technique, much the same as OFDM is an orthogonal frequency multiplexing technique. Furthermore, we compare the two multiplexing methods with respect to their characteristics like spectral efficiency (SE) and peak-to-average power ratio (PAPR). We then demonstrate real-time Nyquist pulse generation for signals beyond 100 Gbit/s. This has become possible even with the limited speed of state-of-the art electronics [4]. In more detail, we generate quadrature phase shift keying (QPSK) at 56 Gbit/s and quadrature amplitude modulation with 16 states (16QAM) at 112 Gbit/s in combination with polarization division multiplexing (PDM). This results in an overall spectral efficiency of 7.5 bit/s/Hz for PDM-16QAM. Finally the reception of Nyquist shaped pulses is discussed comparing it with the reception of standard non-return-to-zero (NRZ) QAM signals.

2. Advanced filtering in optical WDM networks

Modern optical networks rely on multi-wavelength and multi-carrier transmission systems in order to fully exploit the bandwidth offered by optical fibers. The ultimate target is to maximize the spectral efficiency, i. e., the amount of transmitted data within a given bandwidth [5]. In general, the maximum capacity of a channel is only limited by Shannon's law. For optical communications non-linear distortions limit the ultimate channel capacity at

#158081 - $15.00 USD Received 14 Nov 2011; accepted 3 Dec 2011; published 20 Dec 2011

high launch powers. Thus increasing the signal to noise ratio (SNR) by increasing the signal power is only possible within certain limits [6, 7]. For high capacity networks, coming close to this so-called non-linear Shannon limit is of special interest.

For conventional *M*-ary QAM signals, the spectral occupancy does not alter significantly when changing the number of bits *b* transmitted per symbol. Thus increasing the number of constellation points $M = 2^b$ leads directly to an increase in spectral efficiency. However, transmitting an additional bit per symbol implies doubling the number of constellation points, so that for a constant average power the required signal-to-noise ratio (SNR) increases significantly. This is also true if the spectral efficiency is increased by polarization division multiplexing (PDM) or polarization switching [8].

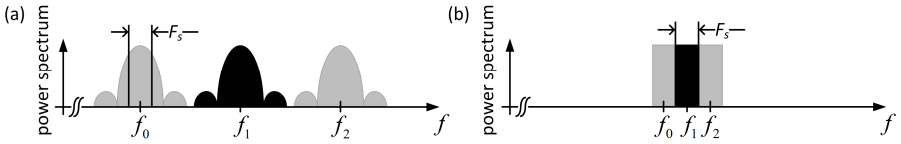

Fig. 1. Reducing the required channel spacing in WDM systems by removing spectral portions outside the Nyquist bandwidth F_s through filtering. Minimum channel spacing for crosstalk free systems is fixed by F_s. (**a**) Unfiltered *M*-ary QAM channels with theoretically infinitely wide spectrum. (**b**) Nyquist channel center frequencies can be spaced apart by the Nyquist bandwidth F_s. Basically, no guard bands are required.

Bandwidth can be saved, however, when applying advanced filtering. From signal theory we know that the minimum bandwidth needed to fully encode a bandwidth-limited signal is the Nyquist bandwidth F_s [9]. If the optimization of spectral efficiency is the ultimate target, all frequency components outside the Nyquist band must be removed by filters. As a consequence, the time domain signal changes from pulses that are clearly separated in time (e. g., non-return-to-zero format, NRZ) to pulses that overlap their neighbors.

As an example, Fig. 1(a) displays the spectrum of an *M*-ary QAM NRZ signal for three different WDM channels centered at optical frequencies f_0, f_1, and f_2. The spectra are significantly wider than F_s, but can be reduced to the Nyquist bandwidth without loosing any signal information. However, appropriate filtering is required to achieve the best possible transmission quality. The sinc-shaped spectrum of an NRZ signal should be filtered such that the resulting spectrum is of rectangular shape under the assumption that the frequency response of the channel is flat in the region of interest. Therefore the side lobes must be removed, and the spectrum within F_s must be flattened. If there are slopes in the channel's frequency response, or the noise accumulated in the system is not constant over frequency, a pre- and de-emphasis filtering scheme should be applied. In a properly filtered WDM spectrum comprising the same three carrier wavelengths as in Fig. 1(a), the channels can now be placed next to each other located on a frequency grid the minimum spacing of which is dictated by the symbol rate F_s (Fig. 1(b), Nyquist-WDM [10, 11]).

In general, the previously described filters can be implemented optically, electrically, or digitally. Possible implementations are shown for a software-defined transmitter, Fig. 2. Optical filters with a transfer function $S_{21}(f)$ as in Fig. 2(a) could be used. The difficulty is to build optical filters with frequency responses that drop significantly inside just a few MHz. Optical filters based on liquid crystals may offer an opportunity to perform such filtering [12]. Nevertheless, these filters are quite elaborate and show some penalties due to the limited slopes in their frequency response. Electrical filters as shown in Fig. 2(b) are another option. They can provide very steep slopes. A complex transmitter, however, requires two filters with a specific frequency transfer function depicted in Fig. 2(b). As before, these analog electrical filters are not easily available. Conversely, designing digital filters to be included in the digital signal processing (DSP) part of the transmitter [13] seems to be a suitable option to solve the problem. State-of-the-art software-defined optical transmitters [14] utilize DSP functionality which only has to be extended. Naturally, digital filtering calls for additional analog anti-aliasing filters to remove image spectra. These filters can be standard low-pass filters as any negative influence can be pre-compensated by digital filtering. Furthermore,

#158081 - $15.00 USD Received 14 Nov 2011; accepted 3 Dec 2011; published 20 Dec 2011

only DSP offers the flexibility to vary filter coefficients during runtime and therefore the capability to adapt to

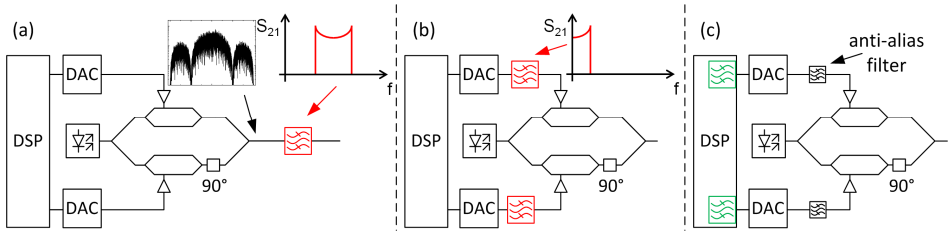

Fig. 2. Pre-filtering of optical *M*-QAM signals for generating sinc-shaped Nyquist pulses. (**a**) An optical filter can be applied to carve an ideal rectangle out of an NRZ spectrum. Such an optical filter requires a frequency response $S_{21}(f)$ that would be difficult – if not impossible – to realize. (**b**) Alternatively, two analog electrical filters can be used to form an appropriate output signal with an ideal rectangularly shaped spectrum. These filters would also need a non-standard transfer function $S_{21}(f)$. (**c**) By digital filtering as a part of the digital signal processing (DSP) block in the transmitter one can efficiently remove redundant parts of the spectrum. Resulting signals show almost ideal rectangular spectra, and additional off-the-shelf analog electrical or optical filters can easily remove spurious spectra.

changes in the channel response. Additionally, changing the symbol rate F_s of the digital filter based transmitter is achieved without changing the hardware. Analog filters are generally fixed with respect to their frequency responses and cannot easily be altered.

3. Nyquist pulse modulation and OFDM: A comparison

Nyquist pulse modulation can be derived from the well-known optical orthogonal frequency division multiplexing (OFDM) technique [1]. This is done by simply interchanging time and frequency domain when describing the signal.

In general, an OFDM signal $x(t)$ is an *infinite* sequence of *temporal* symbols $x^{(i)}(t)$ superscripted with i. Each temporal symbol consists of a superposition of N *temporal sinusoidals* with equidistant carrier frequencies f_k inside a temporally rectangular window defining the temporal symbol length T_s. Frequency spacing $F_s = f_{k+1} - f_k = 1 / T_s$ and temporal symbol length T_s are interrelated to establish orthogonality, Eq. (13) in the Appendix. To simplify the discussion, we let aside a possible cyclic prefix that would reduce the symbol rate below F_s, and would therefore increase the temporal symbol spacing to a value larger than T_s. The OFDM carriers are encoded with complex coefficients c_{ik}. We find for the OFDM signal

$$x(t) = \sum_{i=-\infty}^{+\infty} x^{(i)}(t), \quad x^{(i)}(t) = \sum_{k=0}^{N-1} c_{ik} x_k(t - iT_s),$$
$$x_k(t) = \mathrm{rect}\left(\frac{t}{T_s}\right) \mathrm{e}^{\mathrm{j}2\pi f_k t}, \quad |f_{k+1} - f_k| = F_s = \frac{1}{T_s}. \tag{1}$$

The rectangular function rect(z) is 1 for $|z| < 1/2$ and zero otherwise, see Eq. (12) in the Appendix. By Fourier transforming Eq. (1) we obtain the frequency domain representation of the i-th temporal OFDM symbol, i. e., a set of N spectral sinc-functions centered at frequencies f_k,

$$X(f) = \sum_{i=-\infty}^{+\infty} X^{(i)}(f), \quad X^{(i)}(f) = \sum_{k=0}^{N-1} c_{ik} X_k(f) \mathrm{e}^{-\mathrm{j}2\pi f i T_s},$$
$$X_k(f) = T_s \,\mathrm{sinc}\left(\frac{f - f_k}{F_s}\right). \tag{2}$$

In contrast to OFDM, the *spectrum* $Y(f)$ of a Nyquist signal is a *finite* sequence of N *spectral* symbols superscripted with i. Each spectral symbol consists of a superposition of *infinitely* many *spectral sinusoidals* with equidistant Nyquist pulse position times t_k ("carrier"

#158081 - $15.00 USD Received 14 Nov 2011; accepted 3 Dec 2011; published 20 Dec 2011

positions) inside a spectrally rectangular window defining the spectral symbol length F_s. Temporal spacing $T_s = t_{k+1} - t_k = 1 / F_s$ and spectral symbol length F_s are interrelated to establish orthogonality, Eq. (14) in the Appendix. The Nyquist "carriers" are again encoded with complex coefficients c_{ik}. In analogy to Eq. (1) we find

$$\begin{aligned} Y(f) &= \sum_{i=0}^{N-1} Y^{(i)}(f), \quad Y^{(i)}(f) = \sum_{k=-\infty}^{+\infty} c_{ik} Y_k(f - iF_s), \\ Y_k(f) &= T_s \operatorname{rect}\left(\frac{f}{F_s}\right) \mathrm{e}^{-\mathrm{j}2\pi f t_k}, \quad |t_{k+1} - t_k| = T_s = \frac{1}{F_s}. \end{aligned} \tag{3}$$

By Fourier transforming Eq. (3) we obtain the time domain representation of the i th spectral Nyquist symbol, i. e., a set of infinitely many temporal sinc-functions centered at times t_k,

$$\begin{aligned} y(t) &= \sum_{i=0}^{N-1} y^{(i)}(t), \quad y^{(i)}(t) = \sum_{k=-\infty}^{+\infty} c_{ik}\, y_k(t) \mathrm{e}^{+\mathrm{j}2\pi i F_s t}, \\ y_k(t) &= \operatorname{sinc}\left(\frac{t - t_k}{T_s}\right). \end{aligned} \tag{4}$$

The relations Eq. (1) - (4) are visualized in Fig. 3. The left column, Fig. 3(a) and (c), describes the time-frequency correspondence for OFDM, while the right column, Fig. 3(b) and (d), relates to Nyquist pulses. The upper rows of each section in Fig. 3 show the time dependency of the signals, while the lower rows refer to the corresponding spectra.

In Fig. 3(a), three temporally sinusoidal subcarriers modulated with $c_{i1} = c_{i2} = c_{i3} = 1$ form a specific OFDM symbol with width T_s and positioned at $t = 0$. The OFDM spectrum is a superposition of three spectral sinc-functions located at frequencies f_{k-1}, f_k, and f_{k+1}, which are separated by F_s. In Fig. 3(b), the superposition of three temporal sinc-functions is seen which are located at times t_{k-1}, t_k, and t_{k+1} and separated by T_s. These Nyquist pulses are modulated with $c_{i1} = c_{i2} = c_{i3} = 1$ and form a specific spectral Nyquist symbol with width F_s and position at $f = 0$. It consists of three spectrally sinusoidal Nyquist "subcarriers". The graphs in Fig. 3(a) and (b) represent Eq. (1) - (4) for $i = 0$, i. e., for an OFDM and a Nyquist symbol positioned at $t = 0$ and $f = 0$, respectively.

If we set $k = 0$, then each of the three OFDM or Nyquist symbols shown here consists of only one temporal zero-frequency ($f_0 = 0$) or spectral zero-time ($t_0 = 0$) "sinusoidal", respectively. For OFDM, the three temporal symbols are positioned at times $(i–1)T_s$, iT_s and $(i + 1)T_s$, Fig. 3(c). The resulting spectrum is located within a sinc-shaped envelope having its first zeros at $–F_s$ and $+ F_s$. Due to the different positions of the temporal symbols we see three spectral sinusoidals within the (green) spectral envelope. For Nyquist pulses, the three temporal sinusoidals inside the (green) sinc-shaped pulse envelope with zeros at $–T_s$ and $+ T_s$ correspond to three spectral symbols positioned at frequencies $(i–1)F_s$, iF_s, $(i + 1)F_s$, Fig. 3(d).

A schematic of OFDM signal and Nyquist pulse generation is given in Fig. 4. The left column, Fig. 4(a) and (c), refers to OFDM, whereas the right column, Fig. 4(b) and (d), describes Nyquist pulse generation. For a better understanding we set one of the summation variables k or i of Eq. (1) - (4) to zero while varying the other one, and we present the signal generation in both frequency and time domain.

For OFDM signal generation in the frequency domain, Fig. 4(a), a real sinc-shaped spectrum $X_{k=0}(f)$ centered at $f = 0$ is shifted by a finite number of equidistant frequency steps kF_s, $k = 0…N–1$. The resulting sub-spectra are modulated by complex coefficients c_{ik}. The total OFDM spectrum $X^{(0)}(f)$ for $i = 0$ is formed by superimposing all N subcarrier spectra (Σ stands for summation), resulting in an OFDM symbol located at $t = 0$ only.

For Nyquist pulse generation in the time domain, Fig. 4(b), a real sinc-shaped impulse $y_{k=0}(t)$ centered at $t = 0$ is shifted by an infinite number of equidistant time steps kT_s, $k = –\infty… + \infty$. The impulses are modulated by complex coefficients c_{ik}. The total Nyquist pulse $y^{(0)}(t)$ for i

#158081 - $15.00 USD Received 14 Nov 2011; accepted 3 Dec 2011; published 20 Dec 2011

= 0 is formed by superimposing all "subcarrier" pulses, resulting in a Nyquist pulse sequence at one carrier "frequency" $f = 0$ only.

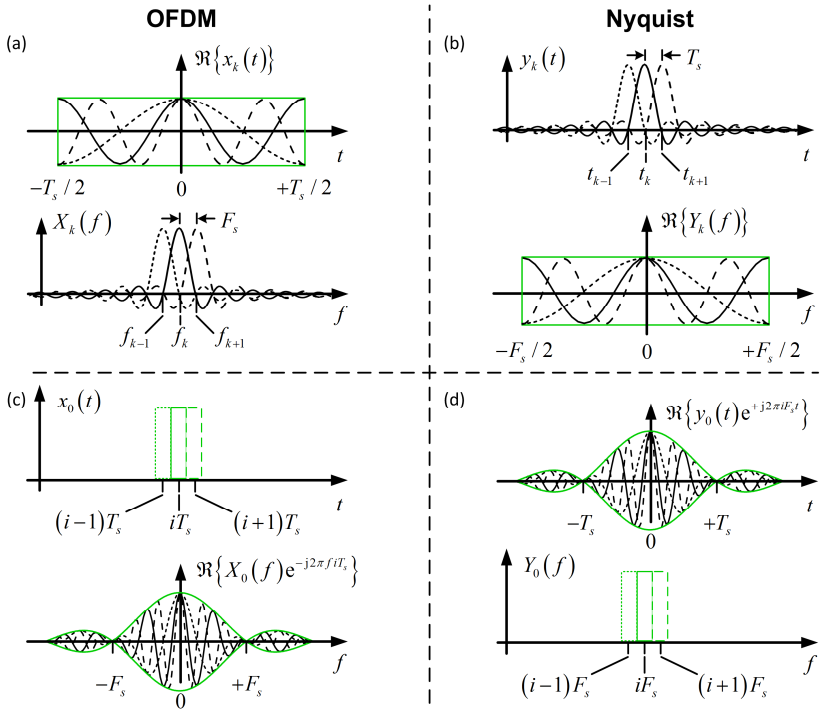

Fig. 3. Comparison between OFDM (left column) and Nyquist sinc-pulses (right column) in time and frequency domain. (**a**) The upper graph shows the real parts of three on-off keyed sinusoidal subcarriers $x_k(t)$, the sum of which represents one specific time-domain OFDM symbol centered at $t = 0$. The lower graph shows the corresponding spectra $X_k(f)$ of the subcarriers centered at frequencies f_{k-1}, f_k, and f_{k+1}. (**b**) The upper graph shows three Nyquist pulses $y_k(t)$ ("temporal subcarriers") centered at times t_{k-1}, t_k, and t_{k+1}. The lower graph shows the corresponding real parts of the spectra $Y_k(f)$ with three spectral sinusoidals, the sum of which represents one specific frequency-domain Nyquist symbol centered at $f = 0$. (**c**) The upper graph shows the envelopes (green rectangles as in Fig. 3(a) of three temporal OFDM symbols located at times $(i-1)T_s$, iT_s, and $(i + 1)T_s$. For simplicity, each temporal OFDM symbol is composed of the same single zero-frequency subcarrier $f_0 = 0$ for $k = 0$, The lower graph shows the corresponding real parts of the spectra within a sinc-shaped envelope (green). The three spectral sinusoidals within correspond to three temporal positions of the temporal OFDM symbol. (**d**) The upper graph shows the real parts of three Nyquist pulses within a sinc-shaped envelope (green). The three temporal sinusoidals within correspond to three spectral positions of the spectral Nyquist symbols. The lower graph shows the envelopes (green rectangles as in Fig. 3(b) of the three spectral Nyquist symbols located at frequencies $(i-1)F_s$, iF_s, and $(i + 1)F_s$. For simplicity, each spectral Nyquist symbol is composed of the same single zero-time Nyquist "subcarrier" $t_0 = 0$ for $k = 0$.

For OFDM pulse generation in the time domain, Fig. 4(c), a real rect-shaped pulse $x_{k=0}(t)$ comprising only one carrier "frequency" $f = 0$ is shifted by an infinite number of equidistant time steps iT_s, $i = -\infty \ldots +\infty$. These sub-pulses are modulated by complex coefficients c_{ik}. The total OFDM time signal $x(t)$ for $f = 0$ is formed by superimposing infinitely many temporal sub-pulses.

For Nyquist signal generation in the frequency domain, Fig. 4(d), a real rect-shaped spectrum $Y_{k=0}(f)$ comprising only one Nyquist pulse ("carrier") at $t = 0$ is shifted by a finite number of equidistant frequency steps iF_s, $i = 0 \ldots N-1$. The resulting sub-spectra are modulated by complex coefficients c_{ik}. The total Nyquist symbol $Y(f)$ at $t = 0$ is formed by superimposing all N sub-spectra.

#158081 - $15.00 USD Received 14 Nov 2011; accepted 3 Dec 2011; published 20 Dec 2011

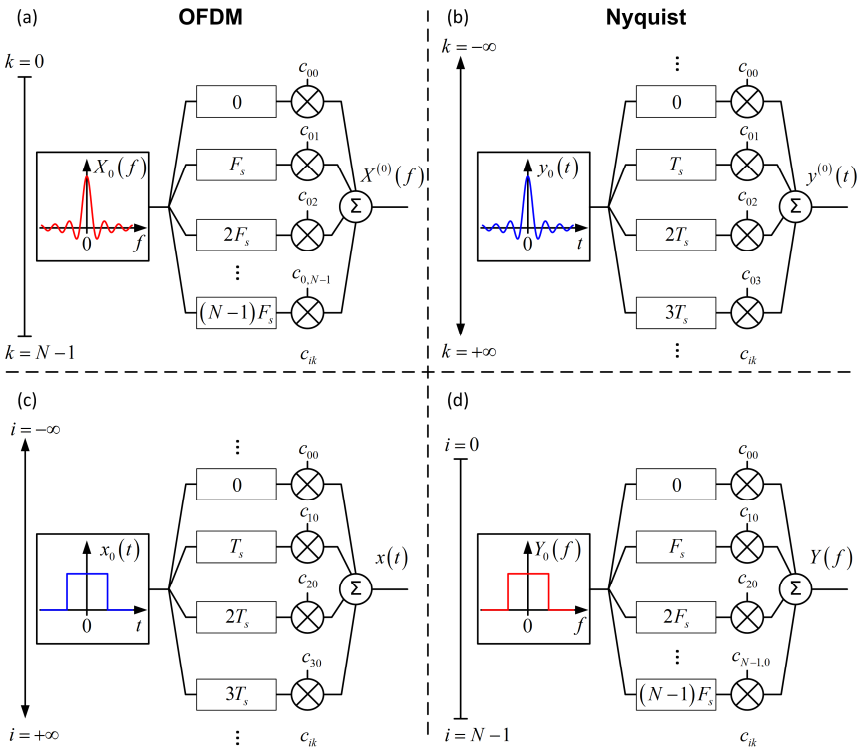

Fig. 4. Schematic of OFDM signal and Nyquist pulse generation, both in frequency domain and time domain. For a better understanding we keep either k or i of Eq. (1) - (4) constant at zero while varying the other quantity. (**a**) OFDM spectrum, OFDM symbol at $t_0 = 0$ ($i = 0$) only: N sinc-shaped sub-spectra for a finite number of $k = 0…N - 1$ keyed subcarriers are frequency shifted by kF_s and modulated with complex coefficients c_{ik}. The superposition of all modulated sub-spectra results in the total OFDM spectrum $X(f) = X^{(0)}(f)$. (**b**) Nyquist pulse, Nyquist symbol with $f_0 = 0$ ($i = 0$) only: Infinitely many sinc-shaped pulses (Nyquist "subcarriers", $k = -\infty… + \infty$) time shifted from $t = 0$ by increments kT_s and modulated with complex coefficients c_{ik}. The superposition of all modulated pulses results in the total Nyquist time signal $y(t) = y^{(0)}(t)$. (**c**) OFDM symbol, OFDM spectrum with $f_0 = 0$ ($k = 0$) only: Infinitely many rect-shaped temporal pulses ($i = -\infty… + \infty$) time shifted from $t = 0$ by increments iT_s and modulated with complex coefficients c_{ik}. The superposition of all modulated pulses results in the total OFDM time signal $x(t)$. (**d**) Nyquist symbol, Nyquist pulse at $t_0 = 0$ ($k = 0$) only: N rect-shaped sub-spectra for a finite number of $i = 0…N - 1$ keyed spectral symbols are frequency shifted by iF_s and modulated with coefficients c_{ik}. The superposition of all modulated spectra results in the total Nyquist spectrum $Y(f)$.

OFDM and Nyquist *receivers* can be built similar to the transmitter scheme depicted in Fig. 4. To this end, the received signal would enter from the right, the symbol Σ would represent a splitter, and local oscillators with complex conjugate time dependency (OFDM signal) or complex conjugate Nyquist pulses (Nyquist signal) mix with the incoming signals to recover the modulation coefficients c_{ik} having integrated over the symbol period T_s (for OFDM signal) or over all times (for Nyquist signals). Forming the complex conjugate means reverting the signs of frequency steps F_s and time steps T_s, respectively.

An in-depth mathematical comparison between OFDM and Nyquist pulse shaping is given in the Appendix. Due to the close relation to OFDM, Nyquist pulse generation could be also referred to as an orthogonal *time* division multiplexing (OTDM) technique.

4. Oversampled Nyquist pulses with finite-length

An elementary Nyquist shaped impulse with minimum spectral width is a sinc-function infinitely extended in time. Real Nyquist pulses, however, need to be approximated by a

#158081 - $15.00 USD Received 14 Nov 2011; accepted 3 Dec 2011; published 20 Dec 2011

finite-length representation. For practical reasons finite impulse response (FIR) filters are used to build the pulse shapes [15, 16]. In addition, for separating the baseband spectrum from its periodic repetitions using realizable filters, oversampling by a factor q (typically q = 1.2, 2, …) is needed. In this paper we have chosen q = 2. This way we will subsequently save FPGA resources since sampling points of adjacent symbols fall onto the same time slot. However, smaller oversampling factors such as q = 1.2 suffice if adequate anti-aliasing filters are available. This would allow us to reduce the required processing speed and DAC sampling rate but comes at the cost of an increased processing complexity.

A suitable FIR filter of order R can be constructed by a sequence of R delay elements T_s / q with T_s = 1 / F_s, and R + 1 taps in-between. The tapped signals are weighed by a number of R so-called filter coefficients h_r and summed up to form the filter output, Fig. 5. A "one-tap" filter with order R = 0 reproduces the filter input.

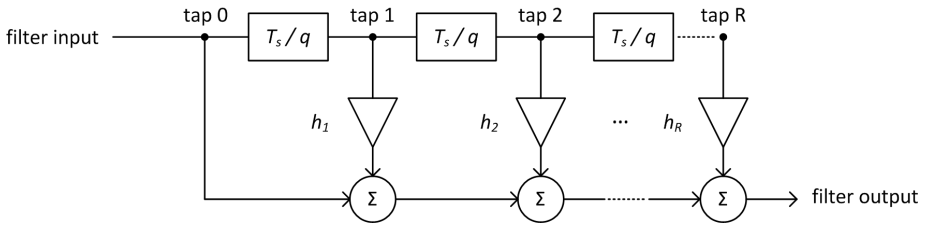

Fig. 5. Finite impulse response filter (FIR, direct form I) of order R. A series of R delay elements T_s / q are located in-between the R + 1 taps. Tapped signals are weighed by R filter coefficients h_r and summed to form the filter output.

Signal generation with various FIR filter orders R is shown in Fig. 6. The left column shows the impulse response of each filter. The effective windowing is indicated by a green rectangle. The linearly scaled corresponding transfer functions are seen in the middle column. The right column displays these same transfer functions on a logarithmic scale. The spectra of the single pulses (white lines) are plotted together with simulated data (colored). A two-fold oversampling q = 2 is used in this context.

The simulation was performed as follows: A pseudo random binary sequence (PRBS) with a length of $2^{15} - 1$ serves as origin for simulated complex data. As a reference, these complex data c_{ik} modulate NRZ pulses, one of which is displayed in Fig. 6(a), left column. The linearly scaled sinc-shaped power spectrum of this elementary impulse is seen in Fig. 6(a), middle column. The logarithm of the same power spectrum is shown as a white line in Fig. 6(a), right column, together with the ensemble-averaged power spectrum for the simulated data. For all power spectra a possibly existent discrete carrier line is omitted.

Nyquist signals shaped with various FIR filters are depicted in Fig. 6(b)-(d). The filter order R with R + 1 taps corresponds to the rectangular time window within which the function is defined (left column, green). The convolution of the rectangular spectrum of an infinitely extended temporal sinc-pulse with the sinc-shaped spectrum of the rectangular time window leads to the power spectra depicted in Fig. 6(b)-(d), middle and right column. As the filter order R increases from R = 16 to R = 1024, the spectrum evolves towards an ideal rectangle rect(f / F_s) with a spectral width equal to the Nyquist bandwidth F_s for complex data. Already for R = 32 a significant increase of the spectral efficiency is to be seen in comparison to NRZ modulation. For R = 1024 the ideal rectangular spectrum is approximated even more closely. However, due to Gibbs' phenomenon, strong ringing at the steep spectral slopes is to be observed. Non-rectangular window functions like Hann or Hamming windows lead to smoothened spectra and a stronger suppression of the side lobes. However, this advantage comes at the price of a widened spectrum and thus a reduced spectral efficiency.

#158081 - $15.00 USD Received 14 Nov 2011; accepted 3 Dec 2011; published 20 Dec 2011

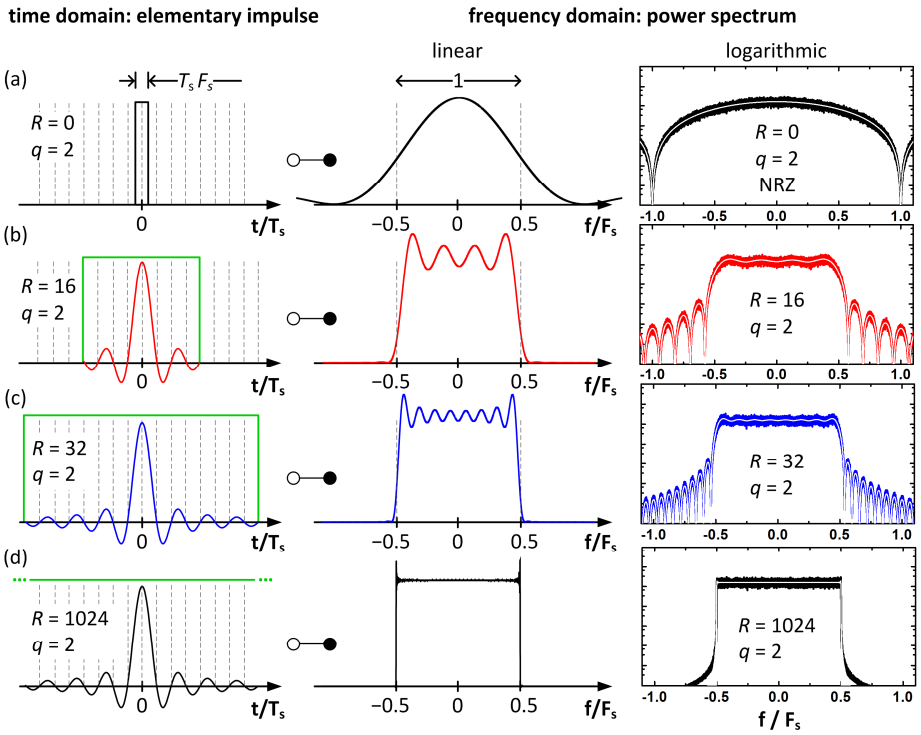

Fig. 6. Impulse responses and transfer functions of FIR filters with various orders R. Left column: Impulse responses. The durations of the impulse response is marked with a rectangular window (green). Middle column: Power spectra on a linear scale. Right column: Power spectra on a logarithmic scale. Colored noisy curves represent the average power spectra for a pulse train with a repetition period $T_s = 1 / F_s$, which has been encoded with random complex data. The white curves reproduce the power spectra from the middle column. For all power spectra a possibly existent discrete carrier line is omitted. (**a**) A single NRZ impulse "shaped" by a one-tap "filter" of order $R = 0$ leads to a sinc-shaped spectrum. (**b**) An ideal sinc-impulse is truncated by a rectangular window. The corresponding filter is of order $R = 16$. The power spectrum results from the convolution of the rect-shaped spectrum of the sinc-impulse with the sinc-shaped spectrum of the rect-window. (**c**) An increased filter order of $R = 32$ leads to a larger time window, and therefore the resulting spectrum evolves towards an ideal rectangular shape. (**d**) A filter with very high order $R = 1024$ closely approximates a rect-shaped power spectrum. Overshoots and ringing are due to Gibbs' phenomenon. All pulses in these plots have been q-fold oversampled with $q = 2$.

5. Spectral efficiency and peak-to-average power ratio

Spectral efficiency (SE) is a major argument for the use of advanced modulation formats in combination with sophisticated multiplexing techniques. Since Nyquist pulses and OFDM signals are closely related, it is interesting to compare the potential SE of both techniques. To this end we compute the spectral width B of the Nyquist pulse up to the first zero outside the main band, which has a width F_s. The same definition is also used for OFDM [1]. The SE results from relating the information rate F_d (measured in bit/s) to the required transmission bandwidth B, SE = F_d / B. Information rate and symbol rate are related as follows: For M-ary single-polarization single-carrier Nyquist pulse transmission, the symbol rate is $F_s^{\mathrm{Nyq}} = F_d / \log_2 M$ (in the Nyquist context abbreviated by $F_s = F_s^{\mathrm{Nyq}}$, see Table 1). For single-polarization M-ary OFDM signals with N subcarriers the symbol rate amounts to $F_s^{\mathrm{OFDM}} = F_d / (N \log_2 M)$ (abbreviated in the OFDM context by the same symbol $F_s = F_s^{\mathrm{OFDM}}$, see Table 1).

#158081 - $15.00 USD
Received 14 Nov 2011; accepted 3 Dec 2011; published 20 Dec 2011

The transmission bandwidth depends on the respective modulation types and formats. For Nyquist pulses, the spectrum is calculated in the Appendix, Eq. (38). Because of the finite length of the actual Nyquist pulses, the spectrum depends on the filter order R and the oversampling factor q, see Fig. 6. For convenience and without loss of generality we choose the spectral symbol $i = 0$ which lies symmetrical to $f = 0$. The spectrum then reads

$$Y^{(0)}(f,R) = \frac{T_s}{\pi}\left[\mathrm{Si}\left(\pi R\frac{f+F_s/2}{qF_s}\right) - \mathrm{Si}\left(\pi R\frac{f-F_s/2}{qF_s}\right)\right]. \tag{5}$$

The function $\mathrm{Si}(z)$ denotes the sine integral [17], see text before Eq. (38) in the Appendix. Power spectra computed from Eq. (5) closely match the graphs of Fig. 6 which are obtained by simulations. To determine the bandwidth $B = B^{\mathrm{Nyq}}$, we find the first spectral zeros to the right and to the left of the main band by a numerically exact evaluation of Eq. (5). From these results we extract a simple empirical relation to estimate the SE of digitally generated Nyquist signals:

$$\mathrm{SE}_{\mathrm{Nyquist}} = \begin{cases} \dfrac{\log_2 M}{1+2.517/R} & \text{for} \quad 1 \le R \le 1024, \;\; q = 2 \\ \log_2 M & \text{for} \quad R > 1024, \;\; q = 2 \end{cases} \tag{6}$$

The resulting spectral efficiency according to Eq. (6) is plotted in Fig. 7(a) (blue line).

For OFDM the SE is influenced by the number of subcarriers N, or in other words by the size of the inverse fast Fourier transform (IFFT) used for signal generation. For our discussion we disregard more advanced OFDM techniques such as a cyclic prefix, guard bands or the introduction of pilot tones that would decrease the SE. The resulting SE then is [1]

$$\mathrm{SE}_{\mathrm{OFDM}} = \frac{\log_2 M}{1+1/N}. \tag{7}$$

The normalized spectral efficiencies of OFDM signals are also depicted in Fig. 7(a) (red line). The SE of both techniques is almost equal.

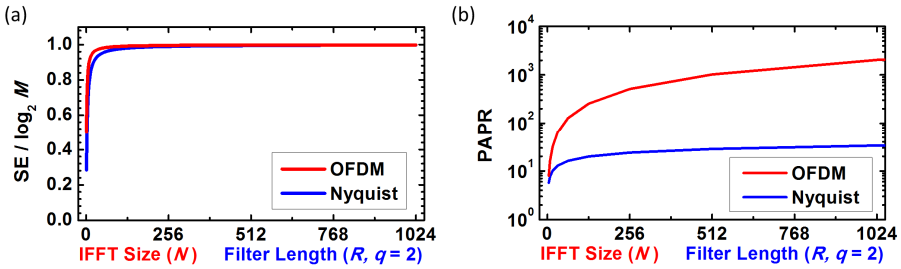

Fig. 7. Spectral efficiency (SE) and peak-to-average power ratio (PAPR) for Nyquist pulses and OFDM signals as a function of the number R of filter taps and the IFFT size N, respectively. (**a**) Normalized spectral efficiency (SE) for single-polarization M-ary QAM modulation. Nyquist shaped signals and OFDM signals show almost identical SE. (**b**) PAPR increases with filter order R for single-carrier Nyquist signals slower than the PAPR for OFDM with the number of subcarriers N.

A major issue that is often referred to reporting on OFDM is the high peak to average power ratio (PAPR) of the time domain signal. This is due to the coherent superposition of multiple sinusoidal carriers that could interfere constructively. As a consequence, high signal amplitudes can occur. In the following we derive PAPR expressions at the transmitter side for Nyquist pulse transmission and for OFDM signaling. At the transmitter, a large PAPR is most critical regarding the rather low resolution of high-speed DACs, the conversion range of which has to be utilized optimally. The PAPR at the receiver end depends heavily on properties of the transmission link like dispersion or nonlinearity tolerance. Therefore, general predictions cannot be made.

#158081 - $15.00 USD Received 14 Nov 2011; accepted 3 Dec 2011; published 20 Dec 2011

To derive an expression for the PAPR in OFDM we need to find the peak power and an expression for the average power. A maximum value can be found as follows: In order to compute the largest possible peak power of an OFDM signal $x(t)$, we assume without loss of generality that the N subcarriers are modulated with a random sequence of real coefficients $c_{ik} = \pm 1$. In this case the maximum amplitude is seen if all N maxima of the temporal sinusoidals happen to add constructively at one point in time, see Fig. 3(a) at $t = 0$ and Eq. (33) in the Appendix. The average power of such a random OFDM signal is the sum of the average powers of the N orthogonal subcarriers. For arbitrary modulation coefficients c_{ik}, the average power for $c_{ik} = \pm 1$ has to be divided by a format dependent factor k^2 [18]. In real-world OFDM systems the infinitely extended ideal spectrum is narrowed by low-pass filtering, so that the orthogonality relation does not hold any more in the strict sense. Nevertheless, with the orthogonality relation Eq. (13) and the power relation Eq. (19) we obtain a good approximation of the average power given by Eq. (36) with $Q = N$. We thus approximate the $\mathrm{PAPR}_{\mathrm{OFDM}}$ by

$$\mathrm{PAPR}_{\mathrm{OFDM}} = \frac{N^2}{\frac{1}{2}N/k^2} = 2k^2N. \tag{8}$$

The result of Eq. (8) for $k^2 = 1$ is seen in Fig. 7(b), red line. With increasing number N of subcarriers the value for $\mathrm{PAPR}_{\mathrm{OFDM}}$ increases linearly. However, the probability that an OFDM signal actually has this peak amplitude decreases with the complexity of the M-ary QAM modulation and with the number N of the subcarriers.

For Nyquist signals the PAPR has to be investigated, too, since a superposition of temporally shifted sinc-pulses, see Fig. 3(b), also produces high signal amplitudes at certain times. We assume again that the Nyquist pulses are modulated with a random sequence of real coefficients $c_{ik} = \pm 1$. Although the local extrema of a single sinc-impulse are not located at times $t / T_s = -0.5, 0.5, 1.5\ldots$, i. e., not in the center of the interval between zeros, it can be shown that the extrema of superimposed Nyquist pulses are located at exactly these times, Eq. (24) in the Appendix. For a worst-case consideration all contributions sum up constructively, so in order to obtain the maximum compound signal we sum up the absolute values of sinc-pulses at $t / T_s = 1 / 2$. If the compound Nyquist signal was constructed with infinitely extended sinc-functions, the maximum signal power would not converge when the number of Nyquist pulses increases. Nevertheless, sinc-functions located far away from the time of summation only contribute little to the sum. For a finite approximation of a sinc-impulse as described in Section 4, only R / q pulses can contribute. Here the filter order R denotes the number of time intervals T_s / q for q-fold oversampling, i. e., R stands for the length of the impulse response. We find the maximum power, see Eq. (25) in the Appendix with $Q = R / q$

$$P_{\max} = \left[\sum_{r=-R/(2q)+1}^{R/(2q)} \left| \mathrm{sinc}\left(\frac{1}{2} - r \right) \right| \right]^2. \tag{9}$$

Technically speaking, $P_{\max}$ could become arbitrarily large for large filter orders R. Yet, while $P_{\max}$ increases with R, the probability for finding R sinc-pulses interfering constructively decreases as well similarly to the OFDM case.

For finalizing the calculation of the PAPR, we need the average power of a single-carrier Nyquist signal $y^{(0)}(t)$ encoded with real coefficients $c_{ik} = \pm 1$. According to [19] we find the average power $\overline{P}$ of an ideal Nyquist signal (see Eq. (21) in the Appendix),

$$\overline{P} = \frac{1}{T_s} \int_{-\infty}^{+\infty} \mathrm{sinc}\left(\frac{t}{T_s} \right) \mathrm{d}t = 1. \tag{10}$$

As for band-limited OFDM spectra, orthogonality is lost for truncated Nyquist sinc-impulses. If Nyquist pulses are generated with a filter of finite (but sufficiently large) order R, orthogonality as implied by Eq. (10) is still a good assumption, so that the average power of truncated Nyquist sinc-impulses is close to $\overline{P} = 1$. As before, for arbitrary modulation

#158081 - $15.00 USD Received 14 Nov 2011; accepted 3 Dec 2011; published 20 Dec 2011

coefficients c_{ik}, Eq. (10) has to be divided by a format dependent factor k^2 [18]. The $\mathrm{PAPR}_{\mathrm{Nyquist}}$ then follows from the ratio of maximum power P_{max} and average power $\bar{P} \approx 1/k^2$,

$$\mathrm{PAPR}_{\mathrm{Nyquist}} = \frac{P_{\max}}{\bar{P}} \approx k^2 \left[\sum_{r=-R/(2q)+1}^{R/(2q)} \left| \mathrm{sinc}\left(\frac{1}{2} - r \right) \right| \right]^2 . \tag{11}$$

A detailed mathematical description is given in the Appendix, leading to Eq. (31). The PAPR of Nyquist signals from Eq. (11) and $k^2 = 1$ is plotted in Fig. 7(b), blue line. Unlike OFDM signals where the PAPR increases linearly, Eq. (8), the PAPR of Nyquist signals does not, due to the temporal decay of its elementary sinc-impulse. However, neither for OFDM nor for single-carrier Nyquist pulses the PAPR converges with increasing IFFT size N or filter order R, respectively.

In Nyquist WDM systems, the PAPR could be higher, because multiple spectral symbols separated by at least F_s might add up constructively as well. However, the Nyquist channel spacing is typically in the order of several GHz [11–13] whereas OFDM carrier spacings are often chosen to be in the MHz [20, 21] range. For large channel spacings as in Nyquist WDM, however, strong signal peaks only occur for very short times, and dispersion causes signal peaks to decay rapidly if large frequency differences are involved. Non-linear effects in WDM systems have been investigated in [22].

6. Implementation

In order to electronically generate Nyquist pulses, advanced digital signal processing (DSP) along with digital-to-analog converters are needed. Suitable devices for high-end DSP are either application-specific integrated circuits (ASIC) or field programmable gate arrays (FPGA). Since ASIC development is time consuming and comes along with high financial efforts, the use of FPGA for prototyping purposes is well established.

6.1 FPGA based DSP

The main challenge for real-time Nyquist pulse generation is the development of high performance FIR filters that provide a sufficient number of filter taps, have adequate precision, and enable a high data throughput. The extensive use of look-up tables (LUT) is a highly efficient way to implement FIR filters on FPGAs, since resource hungry complex multiplications can be avoided. The principle scheme of the DSP performed by the FPGA is depicted in Fig. 8. Due to the strong parallelization of the processing, the FPGA internal clock can be significantly lower than the Nyquist pulse rate. The FPGA produces 128 samples (each

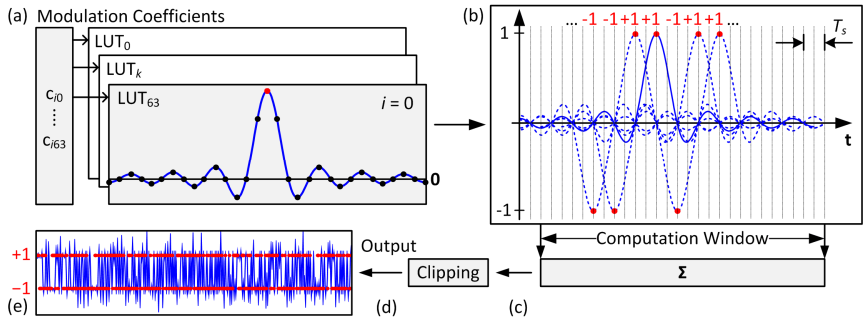

Fig. 8. FPGA parallel processing. In each computation window the FPGA produces a series of 64 sinc-pulses with different weighting coefficients $c_{ik} = \pm 1$ and for $i = 0$. (**a**) Products of modulation coefficients and windowed sinc-pulses (two-fold oversampled, $q = 2$) are stored within 64 lookup tables (LUT). Stored samples within the LUT are marked as dots. Each of the 64 LUT outputs is delayed in time such that (**b**) sinc-maxima (red dots) fall on the zeros of neighboring sinc-functions corresponding to a spacing by T_s. For each of the 128 sampling times inside the computation window the non-zero samples are added (**c**), clipped (**d**), and eventually produce the output waveform (**e**).

#158081 - $15.00 USD Received 14 Nov 2011; accepted 3 Dec 2011; published 20 Dec 2011

of 6 bit depth) per clock cycle (4.57 ns for 28 GSa/s). In each computation window (and for an oversampling factor of $q = 2$), a series of 128 / 2 = 64 modulated sinc-pulses form the output signal, Fig. 8. The FIR filter is realized in the time domain by convolving the complex modulation coefficients c_{ik} with a sampled sinc-shaped impulse. All possible products of c_{ik} and an elementary sinc-impulse are sampled (dots in Fig. 8(a)), quantized and stored within LUTs. For illustration purposes we choose $c_{ik} = \pm 1$ as coefficients for the spectral symbol $i = 0$. The LUT outputs are delayed by a multiple of T_s, Fig. 8(b), and all samples belonging to the same point in time are added, Fig. 8(c). The resulting output is fed to a clipping module, Fig. 8(d), which then delivers the output Nyquist waveform as seen in Fig. 8(e). Red dots mark the position of the sinc-pulse maxima ± 1. Continuous operation for an infinite number of Nyquist pulses is achieved through cyclic buffering of samples that are used within adjacent computation windows.

6.2 Experimental setup

Our real-time Nyquist pulse transmitter (Tx) comprises two Xilinx Virtex 5 field programmable gate arrays (FPGA), two high-speed Micram DACs with 6 bit resolution, a nested $LiNbO_3$ Mach-Zehnder modulator (MZM) serving as an I/Q-modulator, and an erbium-doped fiber amplifier (EDFA). We modulate a continuous wave (CW) external cavity laser (ECL) with in-phase (I) and quadrature-phase (Q) data as shown in Fig. 9. Within the FPGAs, complex Nyquist pulses are calculated from a $2^{15} - 1$ PRBS in real-time as outlined above, and passed on to the DACs. The polarization division multiplexing (PDM) stage then emulates a polarization multiplexed signal [2].

We use two complex samples in each symbol time slot leading to a symbol rate of 14 GBd for 28 GSa/s operating DACs. The resulting oversampling by a factor of $q = 2$ can be reduced if adequate electrical or optical anti-aliasing filters are available.

An amplified spontaneous emission (ASE) source adds optical noise to the signal. The noise power can be adjusted by a variable optical attenuator (VOA). A second VOA is used to additionally attenuate the signal when measuring very low optical signal-to-noise ratios (OSNR). An optical band-pass filter removes noise components outside the signal spectrum.

At the receiver (Rx) the signal is split in two. One part feeds an optical spectrum analyzer (OSA) that measures OSNR values for different levels of noise loading. The other part is amplified by an EDFA before it is detected by an Agilent optical modulation analyzer (OMA). The OMA performs the offline processing including carrier phase and clock recovery as well as decoding, bit error ratio (BER), and error vector magnitude (EVM) measurements.

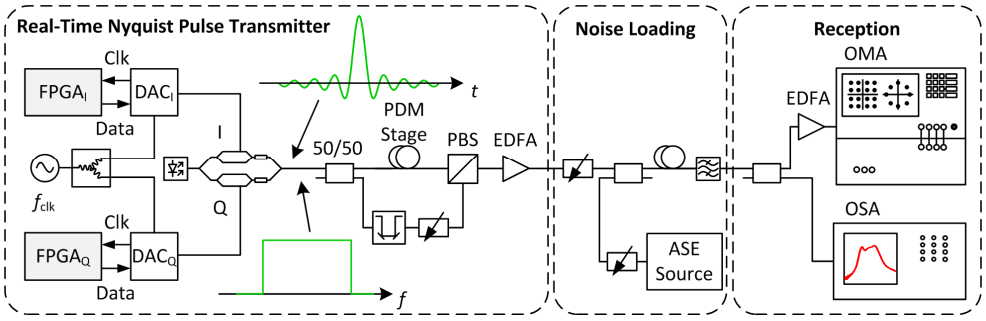

Fig. 9. Experimental setup for a real-time Nyquist pulse transmitter comprising $FPGA_{I,Q}$ and $DAC_{I,Q}$, an externally coupled laser (ECL), an optical I/Q-modulator and an EDFA. An "ideal" elementary output pulse along with its corresponding spectrum is shown as an inset (green). The PDM stage emulates polarization division multiplexing. The signal is loaded with noise by adding a variable amount of amplified spontaneous emission (ASE). The receiver comprises an EDFA along with an Agilent N4391A optical modulation analyzer (OMA) for BER and EVM measurements, and an optical spectrum analyzer (OSA) for OSNR measurements.

#158081 - $15.00 USD Received 14 Nov 2011; accepted 3 Dec 2011; published 20 Dec 2011

7. Experimental results

We performed measurements with PDM-QPSK and PDM-16QAM signals pre-shaped by FIR filters with order 16 and 32 as well as raw NRZ for various levels of OSNR. Measured spectra (colored, noisy curves) for both filters and raw NRZ (black) are seen in Fig. 10(a). The results are consistent with simulations of the FPGA's VHDL code using the ModelSim software (white lines). As expected, the signals generated with R = 32 showed best spectral efficiency and a nearly rectangular shape. The noise floor outside the main band is mostly due to quantization noise (6 bit DAC resolution). Quantization noise does not significantly degrade

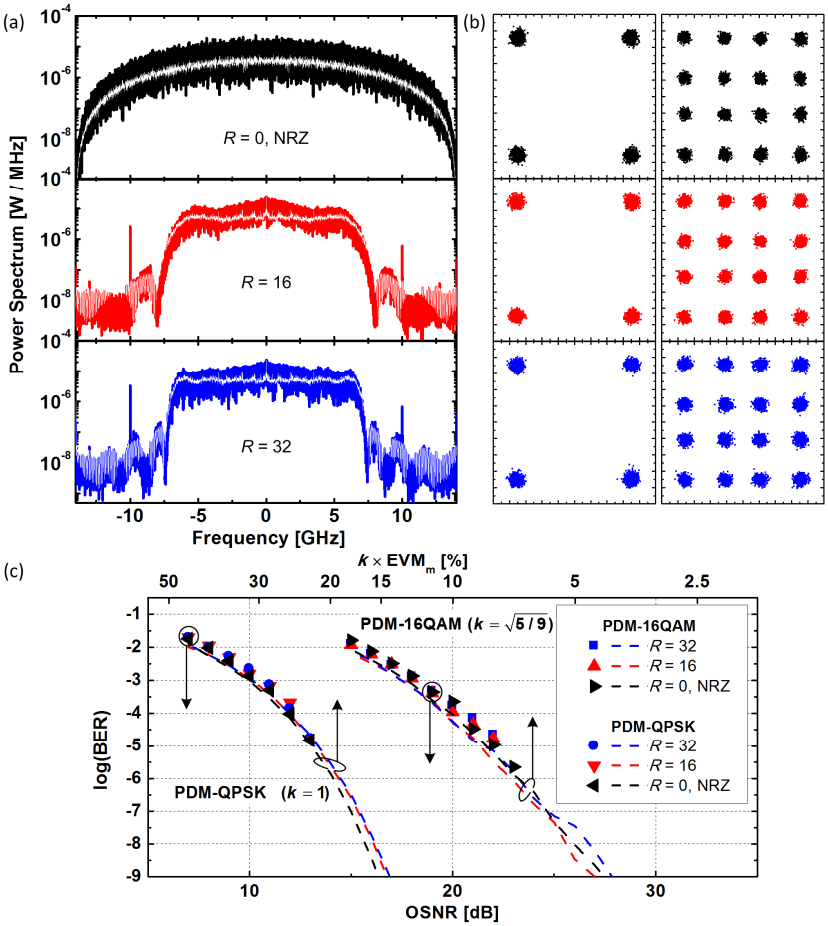

Fig. 10. Spectra, constellation diagrams and BER versus OSNR and EVM results for PDM-16QAM and PDM-QPSK signals generated with R = 0 (black, raw NRZ), R = 16 (red), and R = 32 (blue) filters. Plotted constellation diagrams comprise data from both polarizations. (**a**) Ensemble averages of measured (black, red, and blue) and VHDL simulated (white) spectra. It may be seen that with an increasing number of taps the spectrum evolves towards an ideal rectangle. The observed noise floors next to the spectra are due to quantization noise and do not significantly degrade the signal quality [11]. (**b**) Constellation diagrams for PDM-QPSK and PDM-16QAM at highest possible OSNR. (**c**) Measured BER (symbols) versus OSNR (lower axis). Calculated equivalent BER [18] derived from measured EVM (dashed lines, upper axis) are plotted for Nyquist signals generated with filter of order 16 and 32 and raw NRZ. Calculated EVM values [18] corresponding to the measured OSNR are specified on the upper axis.

the signal quality when the transmitter is employed in a Nyquist WDM system [11], but choosing too small a filter order R deteriorates the signal severely. The displayed constellation

#158081 - $15.00 USD Received 14 Nov 2011; accepted 3 Dec 2011; published 20 Dec 2011

diagrams are constructed by overlaying the diagrams for both polarizations. The results for both filter orders and NRZ are depicted in Fig. 10(b). In order to evaluate the signal quality, the OMA measures BER (symbols in Fig. 10(c)) and EVM. The EVM values are converted to a BER estimate (dashed lines in Fig. 10(c)) according to [18]. The format-dependent factor k, see Eq. (8), and (11), converts an EVM defined by the outermost constellation point (EVM_m) to an EVM defined by the average power (EVM_a) [18]. EVM and OSNR are approximately related by $k \times \mathrm{EVM}_m \approx 1/\sqrt{\mathrm{OSNR}}$ [18]. The measured function BER(OSNR) (symbols, lower horizontal axis) and the estimated function BER(EVM) (dashed lines, upper horizontal axis) are plotted in Fig. 10(c). The graph shows good agreement between measured BER and estimated BER over a broad range. We see no degradation of the signal quality comparing the pulse sequences generated by filters with order 16 and 32 and NRZ. The spectral efficiency for PDM-16QAM (R = 32) is 7.5 bit/s/Hz compared to the theoretical limit of 8 bit/s/Hz.

8. Nyquist pulse reception – required electrical bandwidth and clock phase recovery

Reception of a Nyquist pulse M-ary QAM signal is similar to the reception of a conventional, unfiltered NRZ signal. The complex-modulated optical field is down-converted to the baseband by a coherent receiver (e. g. 90° hybrids with balanced photo-detectors). The electrical signal is then sampled by analog-to-digital converters (ADC) before being processed in the digital domain. Despite all similarities we identified two differences when receiving Nyquist pulses as are discussed in the following.

8.1 Receiver bandwidth impact

Electrical bandwidth is one major limitation for high-speed signal converters (DACs and ADCs) today. An increase of sampling rate, however, is usually achieved by multiplexing multiple low-speed converters. Hence a high sampling rate is not out of reach, whereas high electrical bandwidth is the much bigger challenge. We want to compare Nyquist signals with standard NRZ signals and the corresponding impact of bandwidth-limited ADCs at the receiver. Therefore we generate two signals, namely a Nyquist signal and an NRZ signal, both with 16QAM modulation at a symbol rate of 14 GBd. Both signals carry the same amount of data (56 Gbit/s). Since the ADCs of our receiver have a fixed analog bandwidth of 32 GHz, we emulate a bandwidth-limited system by applying a digital low-pass filter. The cut-off frequency of this flat-top FIR filter is varied from the minimum Nyquist bandwidth 7 GHz up to 9.33 GHz. A qualitative result is seen in Fig. 11. The Nyquist signal shows a very clear constellation diagram even at a receiver bandwidth as low as 7 GHz, Fig. 11(a). The NRZ signal performs poorly under the same conditions, Fig. 11(b). Increasing the bandwidth to 9.33 GHz improves the signal quality of the NRZ, Fig. 11(c). Nonetheless the Nyquist signal outperforms the NRZ signal in all cases.

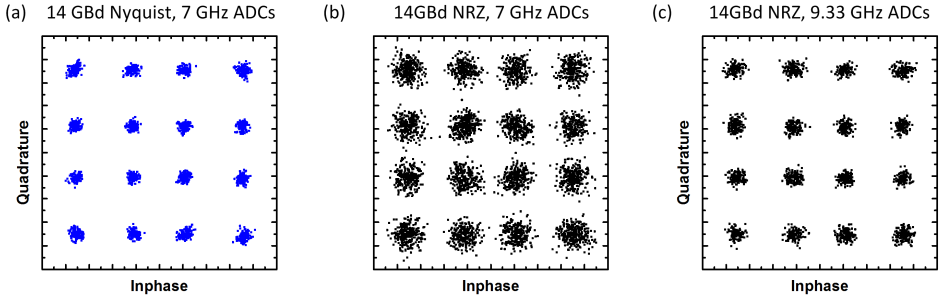

Fig. 11. Constellation diagrams for Nyquist and NRZ signals received with different bandwidths. (**a**) A 14 GBd Nyquist signal is well received with a Nyquist bandwidth of 7 GHz. (**b**) An NRZ of 14 GBd performs poorly with ADCs bandwidth-limited to 7 GHz. (**c**) Increasing the bandwidth to 9.33 GHz enhances the reception of the NRZ signal. Nevertheless, the Nyquist signal shows best performance.

#158081 - $15.00 USD Received 14 Nov 2011; accepted 3 Dec 2011; published 20 Dec 2011

8.2 Clock phase recovery

Careful and proper clock recovery is essential for a solid communication link. In order to investigate the influence of the clock phase for close-to-ideal Nyquist signals we replaced the real-time transmitter, Fig. 9, with an arbitrary waveform generator (AWG). With this transmitter we increased the filter order to 1024, Fig. 6(d).

For standard NRZ and raised-cosine shaped QAM signals it is common to square the signal [12] and perform a fast Fourier transform (FFT) over several received symbols. The outcome of this procedure is illustrated in Fig. 12(a). Next to the DC peak we identify two additional peaks with the frequency of the symbol rate. The spectral location of these peaks reveals the symbol rate, and the phase tells the optimum sample time. Squaring the modulated sinc-shaped pulses and performing an FFT leads to Fig. 12(b). It is obvious that the clock peaks have vanished. Therefore this clock recovery method cannot be applied to sinc-shaped Nyquist signals. Instead we developed an alternative technique to recover the clock phase of a Nyquist signal. In this technique it is sufficient to compute the standard deviation of the modulus of the received Nyquist pulses as a function of the sampling phase. The optimum sampling phase is found when the standard deviation is minimum given that sampling is always done at equivalent positions of subsequent pulses, see Fig. 12(c). Measured (solid lines) and noiseless signals (dashed lines) agree very well. For QPSK, the so computed standard deviation drops to zero for noiseless signals, see Fig. 12(c) (QPSK, dashed line). Accumulated noise in measured signals (solid lines) leads to a vertical shift of the curves' minima. Nonetheless, the minimum standard deviation for all signals can be clearly identified.

The algorithm has been tested and works for QPSK to 256QAM and any intermediate *M*-ary QAM. Since this method neglects the phase of the complex received signal it can be applied prior to carrier phase recovery. Hence standard algorithms for carrier phase recovery can be employed. The influence of a phase error on the signal quality (here represented by EVM) is depicted in Fig. 12(d). Once the optimum clock phase is found, a feedback control minimizing the signal's EVM is perfectly suited even for real-time systems.

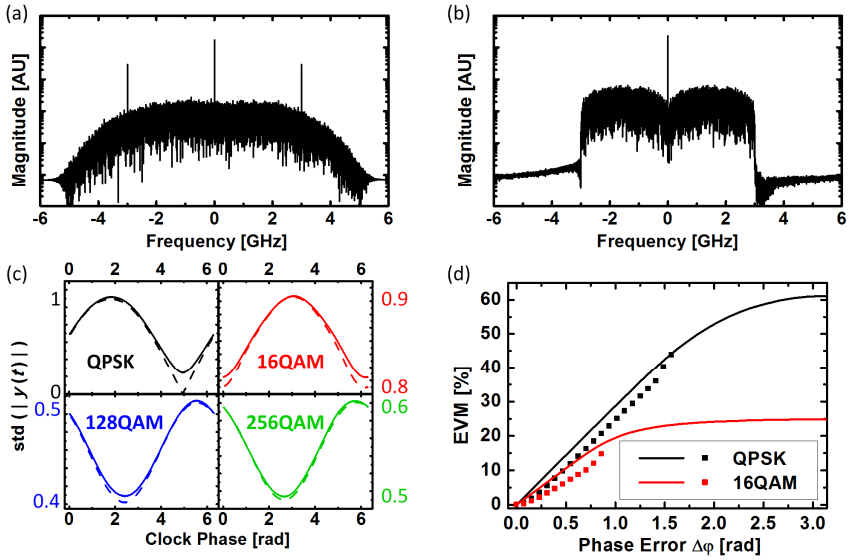

Fig. 12. Clock phase recovery for *M*-QAM modulation of raised-cosine and Nyquist pulses, respectively. (**a**) Spectrum of a squared raised-cosine signal. The clock phase can be extracted from the peaks at the symbol rate. (**b**) Spectrum of a squared Nyquist sinc-pulse train. The peaks at the symbol rate have vanished. (**c**) Standard deviation of the modulus of four measured (solid lines) and noiseless (dashed lines) Nyquist signals plotted over the sampling clock phase. Noise leads to a vertical shift of the curves' minima. The initial points of the graphs are arbitrary and depend on the timing of the data acquisition. (**d**) Dependence of Nyquist signal quality on the clock phase error. Solid line: simulation; squares: measurement.

#158081 - $15.00 USD Received 14 Nov 2011; accepted 3 Dec 2011; published 20 Dec 2011

Accumulated chromatic dispersion (CD) in uncompensated transmission links is usually electrically compensated by a digital filter placed in front of subsequent processing blocks. It is independent of the clock phase recovery described here. Nevertheless, our clock phase recovery algorithm was measured to tolerate a residual dispersion of up to 2400 ps / nm for a 14 GBd QPSK sinc-shaped signal. Furthermore, we found by evaluating transmission experiments, that polarization mode dispersion (PMD) has only negligible influence on the performance of the algorithm.

9. Conclusions

We discussed the correspondence between OFDM and single-carrier Nyquist signals in the time and frequency domain. We introduced a practical implementation of real-time Nyquist signal generation based on FPGA empowered DSP. Both multiplexing techniques have been compared with respect to spectral efficiency and peak-to-average power ratio. We further discussed the implementation and demonstration of a real-time software-defined Nyquist pulse transmitter for data rates up to 112 Gbit/s (PDM-16QAM). The obtained spectra are of rectangular shape, and the signal energy is highly confined to the Nyquist frequency band F_s. Finally, reception of Nyquist signals is explained and demonstrated, pointing out similarities and differences to standard NRZ reception techniques.

Appendix

At this point we want to describe in mathematical detail the properties of Nyquist signals and illustrate their close relation to OFDM. For a better understanding, Table 1 presents an overview of frequently used symbols contrasting OFDM-specific to Nyquist-specific parameters. As usual, the symbols t and f stand for time and frequency.

Table 1. Commonly used terms for OFDM and Nyquist signal description

	OFDM		**Nyquist**
T_s	temporal width of symbol	F_s	spectral width of symbol
F_s	spectral subcarrier spacing	T_s	temporal subcarrier spacing
f_k	spectral subcarrier position	t_k	temporal subcarrier position
$k = 0 \ldots N-1$	index for spectral position of subcarrier (sinusoidal in time)	$k = -\infty \ldots -\infty$	index for temporal position of subcarrier (sinusoidal in frequency)
$i = -\infty \ldots +\infty$	index for temporal position of symbol (rectangular in time)	$i = 0 \ldots N-1$	index for spectral position of symbol (rectangular in frequency)

For general usage we introduce a new set of variables z, Z, m, and Q since the equations can be related either to OFDM or Nyquist signals in frequency or time domain, whichever is of interest. First we define a rectangular window and a sinc-function by

$$\operatorname{rect}\left(\frac{z}{Z}\right) = \begin{cases} 1 & \text{for} \left|z\right| < Z/2 \\ 0 & \text{else} \end{cases}, \quad \operatorname{sinc}\left(\frac{z}{Z}\right) = \begin{cases} 1 & z = 0 \\ \dfrac{\sin\left(\pi z / Z\right)}{\pi z / Z} & z \neq 0 \end{cases}. \tag{12}$$

In the following we summarize the mathematical relations that hold in general:

Orthogonality relations

$$\frac{1}{Z}\int_{-Z/2}^{+Z/2} \mathrm{e}^{\mathrm{j}2\pi m z/Z}\, \mathrm{e}^{-\mathrm{j}2\pi m' z/Z}\, \mathrm{d}z = \delta_{mm'} \qquad \text{for} \qquad m, m' \in \mathbb{Z} \tag{13}$$

$$\frac{1}{Z}\int_{-\infty}^{+\infty} \operatorname{sinc}\left(\frac{z}{Z} - m\right) \operatorname{sinc}\left(\frac{z}{Z} - m'\right) \mathrm{d}z = \delta_{mm'} \qquad \text{for} \qquad m, m' \in \mathbb{Z} \tag{14}$$

#158081 - $15.00 USD Received 14 Nov 2011; accepted 3 Dec 2011; published 20 Dec 2011

Series expansions

We expand functions $\varphi(z)$ in a series of orthogonal complex harmonics with the help of the orthogonality relation Eq. (13), and functions $\psi(z)$ in a series of orthogonal sinc-functions observing the orthogonality relation Eq. (14),

$$\varphi(z) = \sum_{m=-\infty}^{+\infty} \varphi_m \, \mathrm{e}^{\mathrm{j}2\pi m z/Z}, \tag{15}$$

$$\varphi_m = \frac{1}{Z} \int_{-Z/2}^{+Z/2} \varphi(z) \mathrm{e}^{-\mathrm{j}2\pi m z/Z} \, \mathrm{d}z \tag{16}$$

$$\psi(z) = \sum_{m=-\infty}^{+\infty} \psi_m \, \mathrm{sinc}\left(\frac{z}{Z} - m\right) \tag{17}$$

$$\psi_m = \frac{1}{Z} \int_{-\infty}^{+\infty} \psi(z) \mathrm{sinc}\left(\frac{z}{Z} - m\right) \mathrm{d}z \tag{18}$$

Power relations

$$\frac{1}{Z} \int_{-Z/2}^{+Z/2} \left|\varphi(z)\right|^2 \mathrm{d}z = \sum_{m=-\infty}^{+\infty} \left|\varphi_m\right|^2, \tag{19}$$

$$\frac{1}{Z} \int_{-\infty}^{+\infty} \left|\psi(z)\right|^2 \mathrm{d}z = \sum_{m=-\infty}^{+\infty} \left|\psi_m\right|^2. \tag{20}$$

Peak power of a sum of sinc-functions

Nyquist signals and OFDM spectra are both described by a sum $s(z)$ of equidistantly shifted sinc-functions, Eq. (17). We are interested in a worst-case estimation of the maximum power $|s_{\max}|^2$. To this end we assume a constant height of all sinc-functions by choosing coefficients $|\psi_m| = 1$ with equal magnitude. The signs of the coefficients ψ_m are then selected such that a maximum $s_{\max}(z_{\max})$ is found at some position $z_{\max}$. We start by expanding the special function $s^{(1)}(z) = 1$ in a series of sinc-functions, Eq. (17). The expansion coefficients ψ_m are calculated to be $\psi_m = 1 \, \forall m$ by evaluating Eq. (18) and observing that [19, Vol. 1, p. 454, formula 3.721 1.]

$$\frac{1}{Z} \int_{-\infty}^{+\infty} \mathrm{sinc}\left(\frac{z}{Z} - m\right) \mathrm{d}z = 1. \tag{21}$$

From Eq. (17) it follows that

$$s^{(1)}(z) = \sum_{m=-\infty}^{+\infty} \mathrm{sinc}\left(\frac{z}{Z} - m\right) = 1. \tag{22}$$

Equation (22) shows that performing a summation of equally spaced sinc-functions with identical weight leads to a value of 1 at any position z. This value can be exceeded by choosing the expansion coefficients ψ_m appropriately. For this it should be noted that the sinc-function flips sign between adjacent intervals bounded by zeros. The maximum value of the sum $s(z)$ is obtained when all sinc-functions have the same sign in the z-interval under consideration. This is true for

#158081 - $15.00 USD Received 14 Nov 2011; accepted 3 Dec 2011; published 20 Dec 2011

$$s(z) = \sum_{m=-\infty}^{+\infty} \psi_m \operatorname{sinc}\left(\frac{z}{Z} - m\right) = \sum_{m=0}^{+\infty} (-1)^m \operatorname{sinc}\left(\frac{z}{Z} - m\right) + \sum_{m=-\infty}^{-1} (-1)^{m+1} \operatorname{sinc}\left(\frac{z}{Z} - m\right), \tag{23}$$

where the coefficients ψ_m have been chosen such that pairs of sinc-functions m = (0, + 1); (−1, + 2); (−2, + 3); … have all a positive sign in the interval $0 < z < Z$. The resulting function $s(z)$ is monotonic in $0 < z < Z$ and symmetrical with respect to $z = Z/2$, so that the superposition of each pair has its maximum at this point, as will be explained in the following.

Consider a function $f(u)$ which is monotonic in an interval $-U < u < +U$ ($U > 0$). In this interval the sum $s_f(u) = f(u) + f(-u)$ has an extremum if $s_f'(u) = f'(u) - f'(-u) = 0$, i. e., for $u = 0$. This result as applied to Eq. (23) means that the maximum is found at the symmetry point $z_{\max} = Z / 2$ of the sum $s(z)$,

$$s_{\max}\left(\tfrac{1}{2}Z\right) = \sum_{m=-\infty}^{+\infty} \left|\operatorname{sinc}\left(\tfrac{1}{2} - m\right)\right| \tag{24}$$

Note that the sum does not converge. However, Eq. (24) also applies to a finite sum with a maximum of Q sinc-functions, from which the maximum power $s^2_{Q,\max}(Z/2)$ can be computed,

$$s_{Q,\max}\left(\tfrac{1}{2}Z\right) = \sum_{m=-Q/2+1}^{Q/2} \left|\operatorname{sinc}\left(\tfrac{1}{2} - m\right)\right| \tag{25}$$

Average power of an oversampled sinc-function

For deriving the average power of a sum of oversampled shifted sinc-functions sinc(qz/Z–m) (oversampling factor q), we expand $\psi(z)$ = sinc(z/Z) Eq. (17), but this time in terms of oversampled sinc-functions sinc(qz/Z–m). We find the expansion coefficients ψ_m = sinc(m/q) according to Eq. (18) and write

$$\psi(z) = \operatorname{sinc}\left(\frac{z}{Z}\right) = \sum_{m=-\infty}^{+\infty} \operatorname{sinc}\left(\frac{m}{q}\right) \operatorname{sinc}\left(q\frac{z}{Z} - m\right). \tag{26}$$

By substituting $\psi(z)$ in the power relation Eq. (20) and by applying the orthogonality relation Eq. (14) we find the average power

$$\bar{P} = \frac{1}{Z}\int_{-\infty}^{+\infty} |\psi(z)|^2 \, dz = \frac{1}{q}\sum_{m=-\infty}^{+\infty} \operatorname{sinc}^2\left(\frac{m}{q}\right) = 1. \tag{27}$$

In real life, oversampling the base functions by a factor q (preferably q = 2) is needed to simplify the filtering of a Nyquist channel. The sinc(z/Z)-function is then represented not by a number of Q base functions as in Eq. (25), but by q Q base-functions, and again orthogonality is lost in the strict sense. Nevertheless we approximate Eq. (26) by

$$\psi(z) = \operatorname{sinc}\left(\frac{z}{Z}\right) \approx \sum_{m=-qQ/2+1}^{+qQ/2} \operatorname{sinc}\left(\frac{m}{q}\right) \operatorname{sinc}\left(q\frac{z}{Z} - m\right). \tag{28}$$

If q Q is large enough, the average power should be still close to 1,

$$P^{(q,Q)} = \frac{1}{q}\sum_{m=-qQ/2+1}^{+qQ/2} \operatorname{sinc}^2\left(\frac{m}{q}\right) \approx 1. \tag{29}$$

In reality we not only have a finite number q Q of base functions, but the so far assumed equal modulus for all expansion coefficients must be modified if QAM modulated signals come into play. In this case, the approximated average power Eq. (29) needs to be divided by

#158081 - $15.00 USD Received 14 Nov 2011; accepted 3 Dec 2011; published 20 Dec 2011

a format dependent factor k^2 [18], which relates the maximum power of the constellation points to the mean power for all constellation points. Therefore we write approximately

$$\overline{P} \approx P^{(q,Q,k)} = \frac{P^{(q,Q)}}{k^2} = \frac{1}{k^2 q} \sum_{m=-qQ/2+1}^{qQ/2} \operatorname{sinc}^2\left(\frac{m}{q}\right) \approx 1. \tag{30}$$

PAPR for a Nyquist signal

The average power in Eq. (30) serves as reference for the PAPR whereas the maximum power is determined by Eq. (25). We obtain

$$\mathrm{PAPR}_{\mathrm{Nyquist}} = \frac{s_{Q,\max}^2\left(\frac{1}{2}Z\right)}{\overline{P}} = k^2 \frac{\left[\sum_{m=-Q/2+1}^{Q/2} \left|\operatorname{sinc}\left(\frac{1}{2}-m\right)\right|\right]^2}{\frac{1}{q}\sum_{m=-qQ/2+1}^{+qQ/2} \operatorname{sinc}^2\left(\frac{m}{q}\right)}. \tag{31}$$

This equation corresponds to Eq. (11) in the main body of this paper.

Peak power of an OFDM symbol

An OFDM symbol with Q sinusoidal carriers constant within a window of width Z be given by

$$s(z) = \sum_{m=1}^{Q} \sqrt{2} \cos\left(2\pi m \frac{z}{Z} + \alpha_m\right). \tag{32}$$

If the phases α_m of the Q carriers are chosen accordingly and all symbols have maximum values, then all amplitudes add up leading to:

$$s_{Q,\max} = \sqrt{2}\, Q. \tag{33}$$

Average power of an OFDM symbol

The average power can be determined with the power relation Eq. (19),

$$\begin{aligned} P^{(Q)} &= \frac{1}{Z}\int_{-Z/2}^{+Z/2} \left|s(z)\right|^2 \mathrm{d}z = \sum_{m=1}^{Q} \frac{2}{Z}\int_{-Z/2}^{+Z/2} \cos^2\left(2\pi m \frac{z}{Z} + \alpha_m\right)\mathrm{d}z \\ &= \sum_{m=1}^{Q} \frac{2}{Z}\frac{1}{2} Z = \sum_{m=1}^{Q} 1 = Q. \end{aligned} \tag{34}$$

Strictly speaking, orthogonality is lost if the OFDM spectrum is truncated as is always the case in reality. Nevertheless, Eq. (34) represents a good approximation for the average power of an OFDM signal comprising a sufficient number of Q subcarriers. Similar to the arguments leading to Eq. (30), the average power in a symbol needs to be divided by a format dependent factor k^2 [18] such that the average power in a symbol is

$$\overline{P}^{(Q,k)} = Q / k^2 \tag{35}$$

PAPR of an OFDM symbol

The PAPR follows by relating Eq. (33) to Eq. (35). We find

$$\mathrm{PAPR}_{\mathrm{OFDM},k=1} = \frac{s_{Q,\max}^2}{\overline{P}^{(Q,k)}} = 2k^2 Q \tag{36}$$

For Eq. (36) the same number of elementary functions was adopted as for Eq. (31).

#158081 - $15.00 USD Received 14 Nov 2011; accepted 3 Dec 2011; published 20 Dec 2011

Spectrum of a Nyquist signal

The spectrum $Y_{\mathrm{FIR}}^{(0)}(f,R)$ of a Nyquist signal having a finite extent in time results from convolving a rectangular spectrum $Y^{(0)}(f)$ of Eq. (3) (representing the spectrum symmetrical to $f = 0$ of an infinitely extended baseband Nyquist sinc-impulse) with a sinc-shaped spectrum $W(f, R)$ (representing the spectrum of a rectangular time window $w(t) = \mathrm{rect}[t / (RT_s / q)]$ which depends on the number of filter taps R and the oversampling factor q),

$$Y_{\mathrm{FIR}}^{(0)}(f,R) = Y^{(0)}(f) * W(f,R) = T_s \,\mathrm{rect}\left(\frac{f}{F_s}\right) * \frac{R}{q} T_s \,\mathrm{sinc}\left(R\frac{f}{qF_s}\right). \qquad (37)$$

On evaluation we find in terms of the sine integral [17] $\mathrm{Si}(z) = \int_0^z (\sin\nu / \nu)\,\mathrm{d}\nu$

$$Y_{\mathrm{FIR}}^{(0)}(f,R) = \frac{T_s}{\pi}\left[\mathrm{Si}\left(\pi R\frac{f + F_s/2}{qF_s}\right) - \mathrm{Si}\left(\pi R\frac{f - F_s/2}{qF_s}\right)\right]. \qquad (38)$$

Acknowledgments

This work was supported by the EU projects ACCORDANCE and EuroFOS, the Xilinx University Program (XUP), Micram Microelectronic GmbH, the Agilent University Relations Program, the German BMBF project CONDOR, the Karlsruhe School of Optics & Photonics (KSOP), and from the German Research Foundation (DFG).